Modification of Densification Mechanisms By The Timing of Mechanical Pressure During Spark Plasma Sintering

David Salamon (journal@salamons.eu)
Brno University of Technology https://orcid.org/0000-0002-3267-5235
Hua Tan
Brno University of Technology: Vysoke uceni technicke v Brne
Haibo Zhang
Huazhong University of Science and Technology School of Material Science and Engineering

Research Article

Keywords: Spark Plasma Sintering, Pressure applying timing, Microstructure, Alumina, Mechanical properties

Posted Date: January 22nd, 2021

DOI: https://doi.org/10.21203/rs.3.rs-149085/v1

Abstract

The application of mechanical pressure during a sintering process is connected with grains sliding and diffusion enhancement. However, the timing of mechanical pressure during the rapid sintering process was not addressed. In the present study, four different timings of mechanical pressure with final pressure 50 MPa starting from the beginning, 600 ℃, 900 ℃ and at sintering temperature, furthermore one pressure-less SPS have been studied during SPS of Nano-Alumina powder (Taimei, Japan) at 1100 ℃, 1150 ℃, 1200 ℃, and 1300 ℃, respectively. The density, hardness, microstructure, and grain size of each sample were measured and calculated carefully. The results show that applying the pressure at 900 ℃ brings high density and small grain size, leading to the best Vickers hardness. The interaction between pressure and vapor, leading to the different vapor transfer rate of the first sintering stage, is considered as a reason for the differences in the microstructure.

Introduction

Spark Plasma Sintering (SPS), also known as Plasma Assisted Sintering (PAS) and Pulsed Electric Current Sintering (PECS), has been utilized and investigated over the decades. It has been reported that the materials sintered by SPS have much better properties than those sintered by conventional methods, which attracts lots of attention all over the world. The three main features of SPS are direct Joule heating, high heating rate, and mechanical pressure during sintering, among which the effect of mechanical pressure on the SPS process has been studied by numerous researchers. Although the maximum pressure is in a standard setting limited by the graphite die (~ 150 MPa), it shows the great influence on the sintering temperature, densification, grain size, and mechanical properties during the SPS process. Anselmi-Tamburini [1] showed the influence of applied pressure on the final density of nano-zirconia in the range from 20 MPa to 150 MPa, but the crystallite sizes were not affected at sintering temperature 1200 °C and dwell time of 5 mins. Anselmi-Tamburini [2] also sintered nano-zirconia and nano-ceria ceramics at extremely low temperatures under the pressure of 1 GPa and overcomes the deleterious effect of powder agglomeration. The fine grain ceramics were prepared in bulk form. Shen [3] obtained nano-alumina under various pressures (50 MPa, 100 MPa, and 200 MPa) and reported full densification at a lower temperature with a pressure of 200 MPa. Similar hardness and fracture toughness were reported for all applied pressures. Additionally, a special design of the sintering die for high maximum pressure was demonstrated. Balima [4] designed and built a new system within a belt type SPS apparatus by using a large volume chamber and different metal calibrants, which enables the high pressure up to 6 GPa. Aim of high-pressure SPS was often to prepare transparent ceramic materials with better optical performance compared with standard SPS. Grasso [5] produced transparent pure alumina (in-line transmission about 64%) with an average grain size of 200 nm under a pressure of 500 MPa. Zhang [6] sintered transparent (in-line transmittance 68%) yttria under a pressure of 300 MPa. Sokol [7] Obtained transparent (transmittance of about 84%) polycrystalline magnesium aluminate spinel under a pressure of 350 MPa.

However, the question of when to apply the mechanical pressure is still confusing many researchers, only a few papers reported the effect of the pressure applying timing on the SPS process. In the study of Chaim and Shen [8], Neodymium-doped yttrium aluminum garnet (Nd-YAG) nanocrystalline powder was sintered by SPS with pressure applied at 1200 ℃ and sintering temperature (1300 ℃, 1400 ℃, and 1500 ℃), respectively. The result showed that the grain size was more coarse and uneven when applying pressure at a high temperature. Makino [9] applied pressure from the room temperature during the sintering of nano-alumina powder, so did the other researchers, and no report on pressure applying timing effect was found in the literature. According to the sintering theory of ceramics, Somiya [10] describes in his book 6 transport mechanisms: surface diffusion, lattice diffusion (from the surface), vapor transport, grain boundary diffusion, lattice diffusion (from the grain boundary) and plastic flow, the first 3 mechanisms are non-densifying mechanisms which produce microstructure change without causing shrinkage, so they happen mostly in the first sintering stage. The other 3 mechanisms are densifying mechanisms which remove material from the grain boundary region leading to shrinkage, so they happen in the second and third stages.

In order to study the effect of applied pressure timing on the sintering mechanisms, different timing of mechanical pressure have been designed based on the expected densification curve of alumina nanocrystalline powder. The nano-alumina powder is widely used in ceramic research and its sintering behavior is representative. These pressure applying timings are: from the beginning of the sintering (room temperature), beginning of the temperature controller (600 ℃, the radiation pyrometer works at 570 ℃), beginning of shrinkage (900 ℃, the beginning of the second sintering stage) and the end of the heating process (at the beginning of dwell period). In addition, a pressureless SPS sintering is also included in the experiments. The final sintering temperatures are 1100 ℃, 1150 ℃, 1200 ℃, and 1300 ℃, respectively. The microstructures and grain sizes were evaluated and measured. The macro Vickers hardness was selected to reflect the mechanical properties due to that it is a crucial property in industry applications. The achieved results were discussed in connection with the sintering mechanism in detail.

Experiment Method

The pure alumina nanocrystalline powder was commercially available from Taimei Chemicals CO., LTD., Japan, the particle size was about 100 nm. The SPS apparatus which we used was Dr Sinter SPS-625 from Fuji Electronic Industrial CO., LTD. Both pressure-assisted and pressureless sintering were conducted during the experiments, the experimental setups are shown in **Fig. 1**. The left side is standard SPS setting which is consisted of graphite spacers and die-punches (diameter 12 mm), while the right side is a pressureless SPS setting which uses a graphite crucible (inner diameter 20 mm) instead of die-punches, and there is a layer of carbon wool between the sample and the inner wall of the crucible to prevent the non-uniform thermal distribution caused by the direct contact between the sample and the crucible. All the graphite units were from MERSEN France Gennevilliers. For the standard SPS, 2.0 g powder was filled into the graphite die, then sintered in the vacuum with a pulse pattern 12:2. The heating rate was set to 100 ℃/min and followed by a dwell time of 2 min. The pressure was 50 MPa (5.6 kN) and applied from the beginning of the sintering (room temperature), beginning of the temperature controller (600 ℃, the

radiation pyrometer works at 570 ℃), beginning of shrinkage (900 ℃), and the end of the heating process (at the beginning of dwell period). The minimum pressure before applying the pressure was 13.3 MPa (1.5 kN), the pressure applying rates were all the same from 13.3 MPa to 50 MPa in 1 minute. The schematic of the pressure regime is shown in **Fig. 2**. The sintering temperatures were 1100 ℃, 1150 ℃, 1200 ℃, and 1300 ℃, respectively. For the pressureless SPS, the green bodies were made by a uniaxial press with a pressure of 25 MPa (green body density 56.2 %) and then transferred into the graphite crucible. The sintering temperatures were the same as the standard SPS. The temperature was measured by a radiation pyrometer (working temperature range: 570 ~ 3000 ℃) which focused on the hole on the outer surface of the graphite die for standard SPS and the outer wall of the graphite crucible for pressureless SPS, respectively. The current, voltage, temperature, displacement, pressure, and vacuum were recorded by a computer every second.

The density was measured by the Archimedes method. The hardness was measured by a THV-30MD digital Vickers hardness tester with a 5.0 kg force and 12 seconds dwell time. Each sample was measured with 5 points. The microstructure was observed by a Scanning electron Microscope (FEI Verios 460L). The grain size was calculated by a statistical method that counted at least 400 grains in the SEM images.

Results

Table 1. Sample names, final sintering temperature, and achieved properties.

Sample name	Pressure regime	Sintering temperature/ ℃	Density/%	Grain size/um	STV. /um	Hardness/ HV5	STV. /HV5
PB-1100	Beginning	1100	81.00	0.128	0.034	1173.8	32.6
PB-1150	Beginning	1150	92.20	0.160	0.039	1682.8	30.1
PB-1200	Beginning	1200	98.14	0.257	0.077	1948.0	33.3
PB-1300	Beginning	1300	99.70	1.347	0.545	1717.8	65.6
P600-1100	600℃	1100	84.57	0.135	0.037	943.2	35.0
P600-1150	600℃	1150	94.78	0.179	0.052	1692	68.9
P600-1200	600℃	1200	98.96	0.198	0.052	1839.6	31.3
P600-1300	600℃	1300	99.95	2.061	0.809	1757.8	65.7
P900-1100	900℃	1100	76.57	0.135	0.040	670.4	25.8
P900-1150	900℃	1150	96.37	0.177	0.047	1955.1	48.8
P900-1200	900℃	1200	97.70	0.205	0.047	1964.0	23.8
P900-1300	900℃	1300	99.60	1.083	0.464	1645.2	52.4
PS-1100	Sintering temperature	1100	71.60	0.131	0.040	406.8	19.7
PS-1150	Sintering temperature	1150	81.62	0.134	0.041	987.0	27.3
PS-1200	Sintering temperature	1200	86.00	0.146	0.042	1241.8	58.2
PS-1300	Sintering temperature	1300	98.39	1.981	0.769	1851.2	33.1
PL-1100	Pressureless	1100	67.51	0.102	0.034	302.8	12.4
PL-1150	Pressureless	1150	71.30	0.122	0.042	390.8	15.0
PL-1200	Pressureless	1200	75.23	0.121	0.042	634.4	9.5

PL-1300	Pressureless	1300	94.23	0.273	0.099	1739.8	43.4

All the data of density, grain size, hardness and sample name of all the samples in the present study are displayed in **Table 1**. In total, there are 20 different samples in this study, and we also repeated some experiments which were abnormal (for example P900-1150). For each sample, we measured density, grain size, and hardness. In order to convey better expression and understanding, each sample has been given a name, for example, P600-1200 stands for the sample that sintered at 1200 ℃ with pressure applied at 600 ℃.

The density curves of all the samples are shown in **Fig. 3**. It is obvious that the densities of PL samples are much lower than the others. Even at 1300 ℃, the sample PL-1300 is still not fully dense (94.23%). The densities of PS samples are higher than those of PL samples but still lower than PB, P600 and P900 samples. At 1300 ℃ the sample PS-1300 starts to be fully dense (98.39%). The density curve of PB, P600 and P900 samples are quite similar. At 1100℃ the highest density is obtained by the sample P600-1100 (84.57%), while at 1150℃ the density of P900-1150 is the highest (96.37%). At 1200℃ and 1300℃, the PB, P600, P900 samples are all close to fully dense and present little difference in density.

Fig. 4 shows the grain size curve and histogram of each sample sintered with different conditions. At 1100 ℃ and 1150 ℃, the grain sizes of all the samples are still very fine, all around 150 ∼200 nm. At 1200 ℃, the grain size of the sample PB-1200 increases to 257 ± 77 nm, the grain sizes of the other samples are also a bit coarser than those of 1100℃, while they are still below 200 nm. At 1300 ℃, the grain size increases dramatically to 5 ∼ 7 times bigger, among which the grain size of P600-1300 and PS-1300 are the biggest with the value of about 2.0 um, the grain size of PB-1300 and P900-1300 are rather low but still as big as about 1.2 um. The finest grain size is the PL sample, it increases only a few hundred nanometers from 1100 ℃ to 1300 ℃.

The hardness curve and histogram are shown in **Fig. 5**. The hardness of PB, P600, and P900 samples increases firstly and then decreases with the increasing temperature, while the hardness of PS and PL samples increases all the time with the increasing sintering temperature. At 1100 ℃, the hardness values from high to low are samples of PB > P600 > P900 > PS > PL, which indicates that the mechanical pressure is applied earlier, the hardness is higher. In other words, the longer the applied mechanical pressure lasts, the higher the hardness obtains. At 1150℃, the highest hardness is the sample P900-1150 with a value of 1955.1 ± 48.8 HV5. The hardness of P0-1150 and P0-1200 are almost the same around 1690 HV5, while the hardness of PS-1150 and PL-1150 are much lower, which are 987.0 ± 27.3 HV5 and 390.8 ± 15.0 HV5, respectively. At 1200℃, the highest hardness is obtained by P900-1200 as well with a value of 1964.0 ± 23.8 HV5, however, it is only a bit higher than that of PB-1200 and P600-1200. The hardness of PS and PL samples are still much lower. At 1300 ℃, the hardness of PB, P600, and P900 samples decreases, while the hardness of PS and PL samples increases as high as the other samples. The hardnesses of these five samples are not much different.

All the grains are quite fine, among which the grain size of PB-1200 is the largest shown in **Fig. 6** (a), PS-1200 and PL-1200 shown in **Fig. 6** (d) and (e) are both the finest. Moreover, from **Fig 6** (a), (b) and (c), the

grains are all equiaxed and polygonal-shaped, only a few micropores are distributed between the grain boundaries. While from **Fig. 6** (d) and (e), the grains are round and partially connected, there are large pores among the structures.

Fig. 7 shows the microstructures of PB-1300, P600-1300, P900-1300, PS-1300, and PL-1300 samples. Compared with **Fig. 6**, all the grains grow much bigger than those sintered at 1200 ℃, except the PL samples, the grain size of which doesn't increase that much. The grain size of P600-1300 (**Fig. 7** (b)) and PS-1300 (**Fig. 7** (d)) are the largest, PB-1300 (**Fig. 7** (a)) is the second largest, and the PL-1300 (**Fig. 7** (e)) is again the finest. From 1200 ℃ to 1300 ℃ the grain size of the PS sample increases the most shown in **Fig. 6** (d) and **Fig. 7** (d). In **Fig. 7** (a), (b), (c) and (d), the grains are equiaxed and nonhomogeneous, the large grains are more than 3 μm, while the fine grains are less than 1 μm. In addition, the micropores are distributed on the grain boundaries, which is more obvious in the PB and P600 samples shown in **Fig. 7** (a) and (b). In **Fig. 7** (e), there are much fewer micropores and becoming polygonal-shaped, however, the large pores are still presented in the microstructure.

Discussion

4.1 The effect of the mechanical pressure

When the mechanical pressure is applied during powder sintering, the higher density will be obtained, which has been widely reported in the hot pressing and SPS studies. As shown in **Fig. 3**, no matter when to apply mechanical pressure, the density is higher than that without mechanical pressure, which is in line with the other researchers' results. It is quite acceptable that the mechanical pressure has both extrinsic and intrinsic effect on the sintering process. The extrinsic effect of mechanical pressure is related to the direct effect on particle rearrangement and the destruction of agglomerates, as described by Onoda and Toner [11] in their study of model particle packings. Nanoparticles can easily form agglomerates due to van der Waal bonds between particles refer to the book of Stokes and Evans [12]. The agglomerates form an inhomogeneous structure in the green body when the powder is compacted, this leads to a low green body density and the larger the agglomerate, the lower its density. Moreover, it has been reported that the grain size distribution transformed by original crystallites is fully determined by the agglomerates size distribution. Therefore, the mechanical pressure helps to create a high green body density compact and fine grain size distribution. In the present experiment results, as shown in **Fig. 3**, the densities of PB, P600, P900 and PS samples are higher than those of PL samples when sintering at the same temperature. Besides that, as shown in Table 1, the sample P600-1150 and PL-1300 have quite similar density 94.78% and 94.23%, respectively, while the grain sizes are different, the grain size of P600-1150 is 179 ± 52 nm, the other one is 273 ± 99 nm. One reason behind these two results is the extrinsic effect of mechanical pressure.

In terms of the intrinsic effect, it attributes to the external driving force for densification, the chemical potential difference at the fundamental level and temperature distribution. The driving force for sintering which is explained in the work of Munir [13] can be expressed as follows:

$$d\rho / (1-\rho)\, dt = B\,(g\,\gamma / x + P) \quad (1)$$

Where ρ is the fractional density, B is a term that includes diffusion coefficient and temperature, g is a geometric constant, γ is the surface energy, x is the parameter that represents a size scale, t is time, and P is the applied external pressure. The first term on the right side of Equation (1) represents the intrinsic driving force for sintering while the second term represents the intrinsic contribution to the driving force by the applied pressure. One other contribution of mechanical pressure is the chemical potential, Jamnik and Raj [14] studied the volume diffusion in the space-change-controlled diffusional creep, the chemical potential can be expressed as:

$$\mu_l = \mu_i - \mathbb{Z}_n\, \Omega_l \quad (2)$$

where μ_l is the chemical potential at a particle interface under a stress, μ_i is the standard chemical potential, $\mathbb{Z}_n$ is the normal stress at the interface, tensile stress is positive while compressive stress is negative, and Ω_l is the atomic volume of the diffusing species. The applied mechanical pressure is compressive stress; hence the chemical potential increases under a mechanical pressure, which in turn increases the driving force for sintering. This also leads to a higher density at the same sintering temperature. The last contribution of mechanical pressure is the temperature distribution. As the pressureless SPS was conducted in a graphite crucible and vacuum atmosphere, the heat transfer was mainly through radiation, while in the standard SPS, the heat was mainly transferred by mixed mechanism, which was more efficient and generated a higher temperature difference between the surface and the center of the sample. This again promotes the driving force for sintering.

4.2 Effect of the pressure applying timing

As we know, the sintering of ceramic powder is divided into 3 stages, Somiya, Aldinger [10] presented in the book that the first stage starts with that the sharply concave necks form between the individual particles. In this stage, the densification is limited and typically only the first 5% of linear shrinkage. The second stage has the microstructure which consists of a three-dimensional interpenetrating network of solid particles and channel-like pores due to the high cudirvatures of the first stage that have been moderated. This stage covers most of the densification and is considered to achieve 5 ~ 10% porosity. The last stage starts when the grain growth becomes significant and the channel-like pores break down into isolate. This stage is normally accounted for the last few percents of porosity, while it is very much difficult to remove that.

As the displacement of graphite die-punch was recorded by the PC during SPS, we noticed that the shrinkage of pure nanocrystalline Alumina powder starts around 900 ℃ (shown in **Fig. 6** and **Fig. 9**), which means the first stage of sintering starts at 900 ℃. Moreover, our results of alumina densification are similar to the research of Makino [9] who reported that TM-alumina (Taimei, Japan) can be fully dense at 1200 ℃ under 30 MPa and at 1150 ℃ under 100 MPa. Therefore, we designed four timings of mechanical pressure: (1) At the beginning of the SPS process, it was from room temperature, known as PB; (2) At the middle between the beginning of SPS and the starting of the sintering stage, 600 ℃, it was

also near the working temperature of radiation pyrometer, known as P600; (3) At the beginning of the sintering stage, it was from 900 ℃, known as P900; (4) At the sintering temperature, it was from the beginning of dwell period, known as PS.

At 1100 ℃, the densities of all the samples were below 90%, it means the second stage of sintering is not finished yet, and the microstructures are all like the network of solid particles and channel-like pores without much grain growth which is shown in Table 1 and also **Fig. 4**. The grain sizes of all the samples are around 130 nm which is only a few tens of nanometer larger than the raw powder. As shown in **Fig. 5**, the hardness of all samples sintered at 1100 ℃ decreases with the order PB, P600, P900, and PS. The hardness is affected mostly by the density before reaching the fully dense, while as seen in **Fig. 3**, the density decreases with the order P600, PB, P900, and PS. The sample PB-1100 has a lower density of 81.0% but higher hardness of 1173 ± 32.6 HV5, conversely, the sample P600-1100 has a higher density of 84.57% but the lower hardness of 943.2 ± 35.0 HV5. This is supposed to be related with the pressure holding time, the PB sample was sintered with mechanical pressure from the beginning, which means the longest pressure holding time. For the PS samples, there was not such mechanical pressure during the heating up period, the mechanical pressure only was only applied during the dwell period and only lasted 1 minute. The lack of enough pressure effect time in the sintering process might be the reason why the PS samples always have lower density compared with the other SPS samples. For the PB, P600 and P900 samples, the situations were much more complex. At the initial heating up period of the SPS process (From room temperature to 900 ℃), there was no shrinkage occurring as we mentioned above, which means only surface diffusion, lattice diffusion (from the surface) and vapor transportation might play a role due to that these 3 sintering mechanisms produce microstructure change without causing shrinkage. For the PB samples, the mechanical pressure was applied from the beginning. The external force makes the particles getting closer to each other, even contact each other by the surface force. This effect narrows or closes the vapor transportation path, which leads to forming numbers of isolated pores between particles, as seen in **Fig. 8**. In the study of Salamon [15], when using pressureless SPS for sintering Si_3N_4, a small amount of SiC grains was distributed over the sample and on the graphite wall. This was formed beside the aimed α-sialon phase in sintered AY-sialon compositions. However, when using standard SPS, free silicon possibly forming by the decomposition of Si_3N_4 was not detected. It proved that mechanical pressure created an isolated environment to prevent the free elements or vapor from coming out of the system. In the standard SPS process, the pressure is applied from an initial pressure (low pressure) to a final pressure (high pressure), the initial pressure can also make the vapor path narrow but partly closed. While when the pressure is increased to high pressure, most of the vapor is isolated in the structure, then it creates numerous micropores. To this point, this effect suppresses the densification rate. On the other hand, the fact that applying mechanical pressure from the beginning helps to form a more homogenous compact due to the longer stress dwell time on each particle contact point, which leads to a homogenous microstructure and higher hardness. The competing effect of these two factors might cause the experiment results that the sample PB-1100 had a lower density but higher hardness than those of sample P600-1100.

At 1150 ℃, the highest density and highest hardness were both obtained by the sample P900-1150 with a value of 96.37% and 1955.1 ± 48.8 HV5, respectively. This experiment result is surprising for that the density of P900 sample increases the most from 1100 ℃ to 1150 ℃, which is about 0.396 %/℃, this is almost 2 times higher than that of PB and P600 samples, which are 0.224 %/℃ and 0.204 %/℃, respectively. The true shrinkage rate of PB, P600, P900 and PS samples is displayed in **Fig. 9**. The displacement recorded by the PC D_{total} is the total displacement of the sample and the graphite conductor. So the true shrinkage displacement of the sample *Ds* can be expressed as follows:

$$Ds = D_{total} - D_{graphite} \quad (3)$$

$D_{graphite}$ is the displacement of the graphite conductor, which is measured by standard SPS with a fully dense sample instead of the powder, then the recorded displacement came only from the graphite. As shown in **Fig. 9**, the shrinkage rates of all the samples start to increase at 900 ℃, among which the shrinkage rate of P900 sample increases faster than the others and the peak shrinkage rate is achieved at about 1030 ℃, while PB and P600 sample obtain peak shrinkage rate at about 1100 ℃, the PS sample gets that at about 1160 ℃. For PB and P600 samples, they had the same condition during the second stage of sintering, hence the densification rate was on the same level. While for the P900 samples, the mechanical pressure was applied from 900 ℃ and the pressure started to be stable at around 1050 ℃ (the pressure applying time is 1 min). From 900 ℃ to 1100 ℃, the '*P*' in the P900 sample in Formula (1) was increasing from 13.3 MPa to 50 MPa, which was lower than the constant 50 MPa of PB and P600 sample. While from 1100 ℃ to 1150 ℃, the pressures of PB, P600 and P900 sample were the same, the formula could be written as:

$$d\rho / dt = B (g \gamma / x + P) (1 - \rho) \quad (4)$$

the densification rate depends on the density of the moment according to the formula, the larger density, the lower the densification rate. Therefore, the densification rate of the P900 sample is the highest from the formula. Besides the theoretical point, at 900 ℃ the densifying sintering mechanisms (grain boundary diffusion and lattice diffusion (from the grain boundary)) start to work, the particles become 'soft', if we start to increase the mechanical pressure at this moment, the dynamic pressure would promote the densifying sintering mechanisms more efficiently than the case that the pressure is increased when the particles are 'hard', that's to say before shrinkage starts.

According to the research of Grasso [16], the pressure also affects the temperature difference between the outer wall and the inner wall of graphite die. In our case, when the mechanical pressure increases from 1.5 kN (13 MPa) to 5.6 kN (50 MPa), the temperature difference between the outer wall and the inner wall of graphite die will decrease about 100 ℃. As the temperature measurement was taken from the outer wall of the graphite die, the temperature of the inner wall could be different at the same measured temperature but different mechanical pressure. However, all the samples were sintered at the same final mechanical pressure, thus the temperature difference can be ignored during our experiments.

At 1200 ℃, the densities of PB, P600 and P900 samples already got a high density, while the density of sample PS-1200 was only 86%. The PB and P600 samples got the highest hardness because of the highest density, while the hardness of the P900-1200 sample was the same as the P900-1150 sample for that the density increased only a bit but the grains grew. In terms of the grain size, all the samples increased a little bit, not degrading the mechanical properties much. Hence the hardnesses of all the samples are all on the same level as shown in **Fig. 5**. The highest hardness is obtained by the sample P900-1200, and the reason is the better microstructure with fewer micropores. For PB and P600 samples, 1200 ℃ is the optical sintering temperature when sintering nano-alumina powder.

At 1300 ℃, the PS sample was finally fully dense. The grains of all samples grew further to over 1.0 μm, among which the P600 and PS samples had the largest grain size of around 2.0 μm. The pores become more obvious in **Fig. 7**, especially in PB and P600 samples, which are marked with red circles. This is because of the isolation effect of the pressure as explained above. While for P900 and PS samples, most of the vapor could be driven out during the second sintering stage, so there are fewer pores in the microstructure. These pores have a negative effect on the densification and mechanical properties. Therefore, at 1150 ℃ only sample P900 achieved a density of more than 95% and displayed better mechanical properties.

For the Spark Plasma Sintering of pure nano-alumina powder, the mechanical pressure timing influences the non-densifying mechanisms, especially the vapor transport. Therefore, if we want to get the optical mechanical performance, playing with pressure timing is an effective way. In our case, applying the pressure at 900 ℃ for pure nano-alumina powder can be fully densified at an extremely low temperature of 1150 ℃ with a fine grain growth of around 177 nm. Meanwhile, there are still some unexplained results in this study, e. g. what the main difference between PB and P600 samples is? We still need to make more research on the effect of pressure to make the knowledge more accurate and detailed.

Conclusion

(1) By the pressure-assisted SPS after increasing mechanical pressure from an initial 13 MPa to 50 MPa at any time, all the samples achieved fully dense at 1200 ℃, while the sample only got 75% density by pressureless SPS at the same temperature.

(2) Applying the pressure at 900 ℃ (beginning of the 2nd sintering stage) for pure nano-alumina powder can be fully densified at an extremely low temperature of 1150 ℃ (50 ℃ lower) with a fine grain size of around 177 nm (80 nm less).

(3) The highest hardness is obtained by sample P900-1200, 1964 HV5. It is possible to get better mechanical performance by using tailored pressure applying timing when sintering ceramic powders by SPS.

(4) The mechanical pressure has a significant effect on the densifying mechanisms: grain boundary diffusion and lattice diffusion (from the grain boundary) for sintering nano-alumina powder. The timing

of mechanical pressure influences the non-densifying mechanisms as well, especially the vapor transport.

(5) Tailoring vapor transport by the timing of the intensity of mechanical pressure was demonstrated on a simple alumina system, however, this tool can be used also in multicomponent systems with even possible higher impact on the final microstructure.

Declarations

Acknowledgment

The authors wish to express their gratitude and sincere appreciation to the authority of The Technology Agency of the Czech Republic, project TE02000162 for financial support. The research has also been financially supported by the Ministry of Education, Youth and Sports of the Czech Republic under the project CEITEC 2020 (LQ1601). CzechNanoLab project LM2018110 funded by MEYS CR is gratefully acknowledged for the financial support of the measurements/sample fabrication at CEITEC Nano Research Infrastructure.

References

1. Anselmi-Tamburini U, Garay J, Munir Z, Tacca A, Maglia F, Spinolo G. Spark plasma sintering and characterization of bulk nanostructured fully stabilized zirconia: Part I. Densification studies. Journal of materials research 2004;19:3255-62.
2. Anselmi-Tamburini U, Garay JE, Munir ZA. Fast low-temperature consolidation of bulk nanometric ceramic materials. Scripta Materialia 2006;54:823-8.
3. Shen Z, Johnsson M, Zhao Z, Nygren M. Spark plasma sintering of alumina. Journal of the American Ceramic Society 2002;85:1921-7.
4. Balima F, Bellin F, Michau D, Viraphong O, Poulon-Quintin A, Chung UC, et al. High pressure pulsed electric current activated equipment (HP-SPS) for material processing. Materials & Design 2018;139:541-8.
5. Grasso S, Kim B-N, Hu C, Maizza G, Sakka Y. Highly Transparent Pure Alumina Fabricated by High-Pressure Spark Plasma Sintering. Journal of the American Ceramic Society 2010;93:2460-2.
6. Zhang H, Kim B-N, Morita K, Yoshida H, Hiraga K, Sakka Y, et al. Fabrication of Transparent Yttria by High-Pressure Spark Plasma Sintering. Journal of the American Ceramic Society 2011;94:3206-10.
7. Sokol M, Kalabukhov S, Dariel MP, Frage N. High-pressure spark plasma sintering (SPS) of transparent polycrystalline magnesium aluminate spinel (PMAS). Journal of the European Ceramic Society 2014;34:4305-10.
8. Chaim R, Shen Z. Grain size control by pressure application regime during spark plasma sintering of Nd-YAG nanopowders. Journal of Materials Science 2008;43:5023-7.

9. Makino Y, Sakaguchi M, Terada J, Akamatsu K. Consolidation of ultrafine alumina powders with SPS method. Journal of the Japan Society of Powder and Powder Metallurgy 2007;54:219-25.
10. Somiya S, Aldinger F, Spriggs RM. Handbook of advanced ceramics: Elsevier; 2003.
11. Onoda GY, Toner J. Fractal Dimensions Of Model Particle Packings Having Multiple Generations Of Agglomerates. Journal Of the American Ceramic Society 1986;69:C278-C9.
12. Stokes RJ, Evans DF. Fundamentals of interfacial engineering: John Wiley & Sons; 1997.
13. Munir ZA, Anselmi-Tamburini U, Ohyanagi M. The effect of electric field and pressure on the synthesis and consolidation of materials: A review of the spark plasma sintering method. Journal of Materials Science 2006;41:763-77.
14. Jamnik J, Raj R. Space-charge-controlled diffusional creep: Volume diffusion case. Journal Of the American Ceramic Society 1996;79:193-8.
15. Salamon D, Shen Z, Šajgalík P. Rapid formation of α-sialon during spark plasma sintering: Its origin and implications. Journal of the European Ceramic Society 2007;27:2541-7.
16. Grasso S, Sakka Y, Maizza G. Pressure Effects on Temperature Distribution during Spark Plasma Sintering with Graphite Sample. Materials Transactions 2009;50:2111-4.

Figures

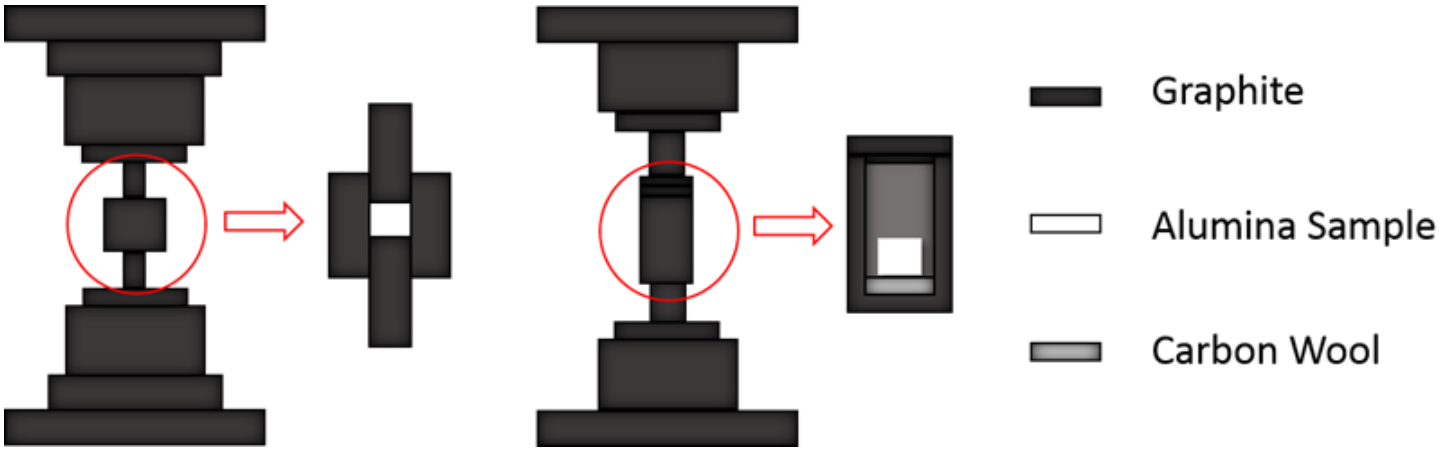

Figure 1

The schematic of both pressure-assisted and pressureless SPS

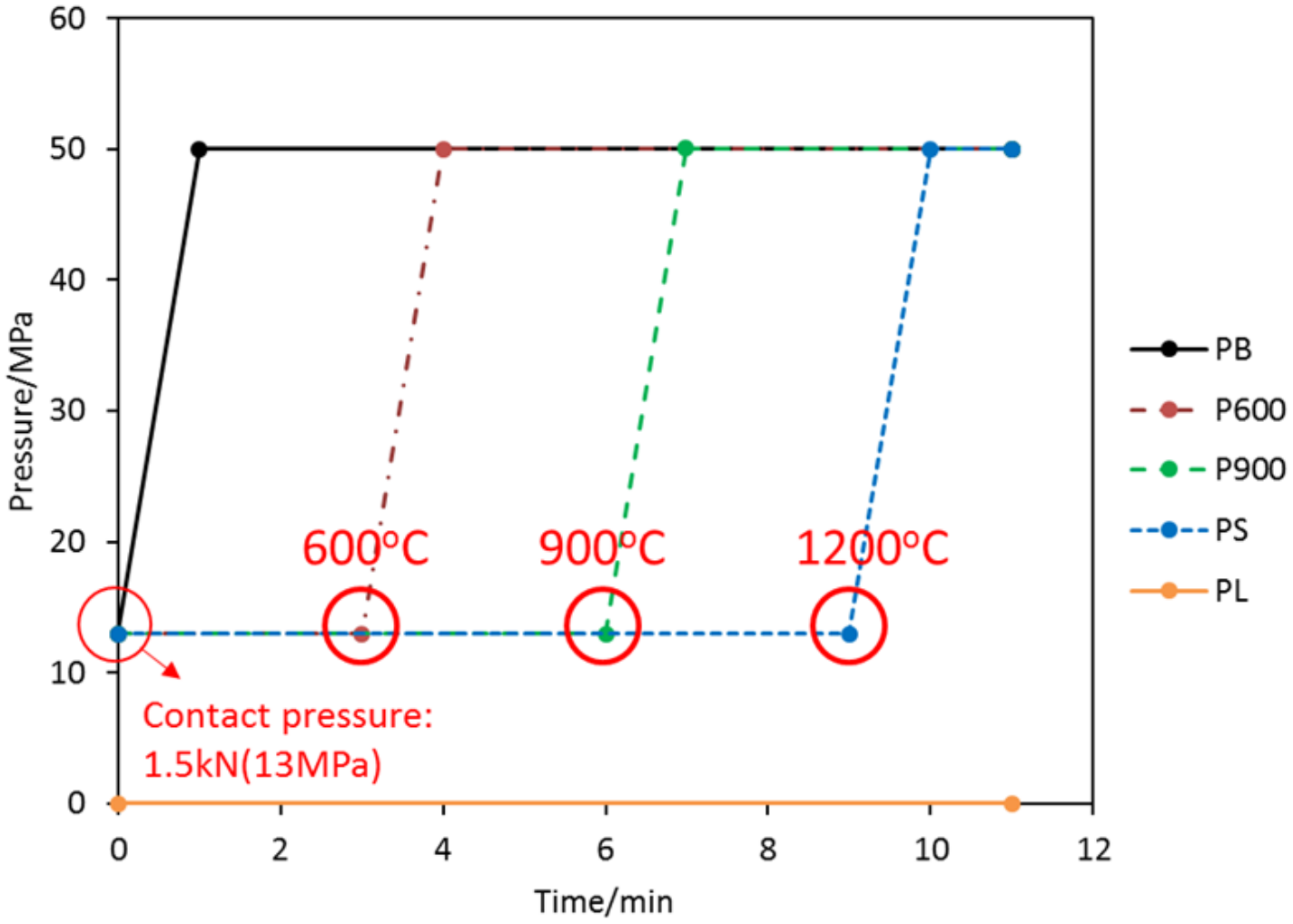

Figure 2

The schematic of the pressure applying timings as the example of sintering at 1200 ℃

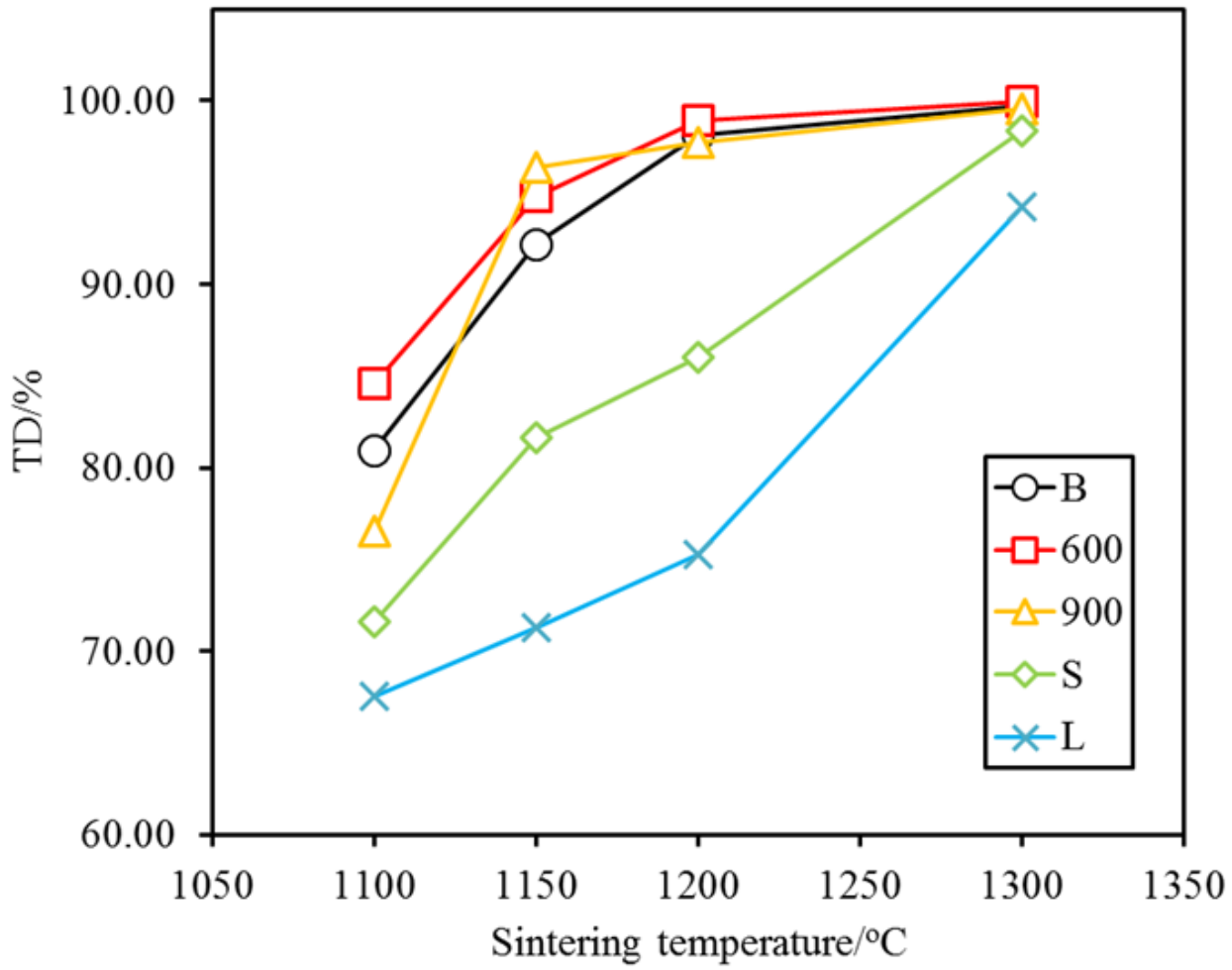

Figure 3

Density curves of samples sintered at different temperature with different pressure applying timings

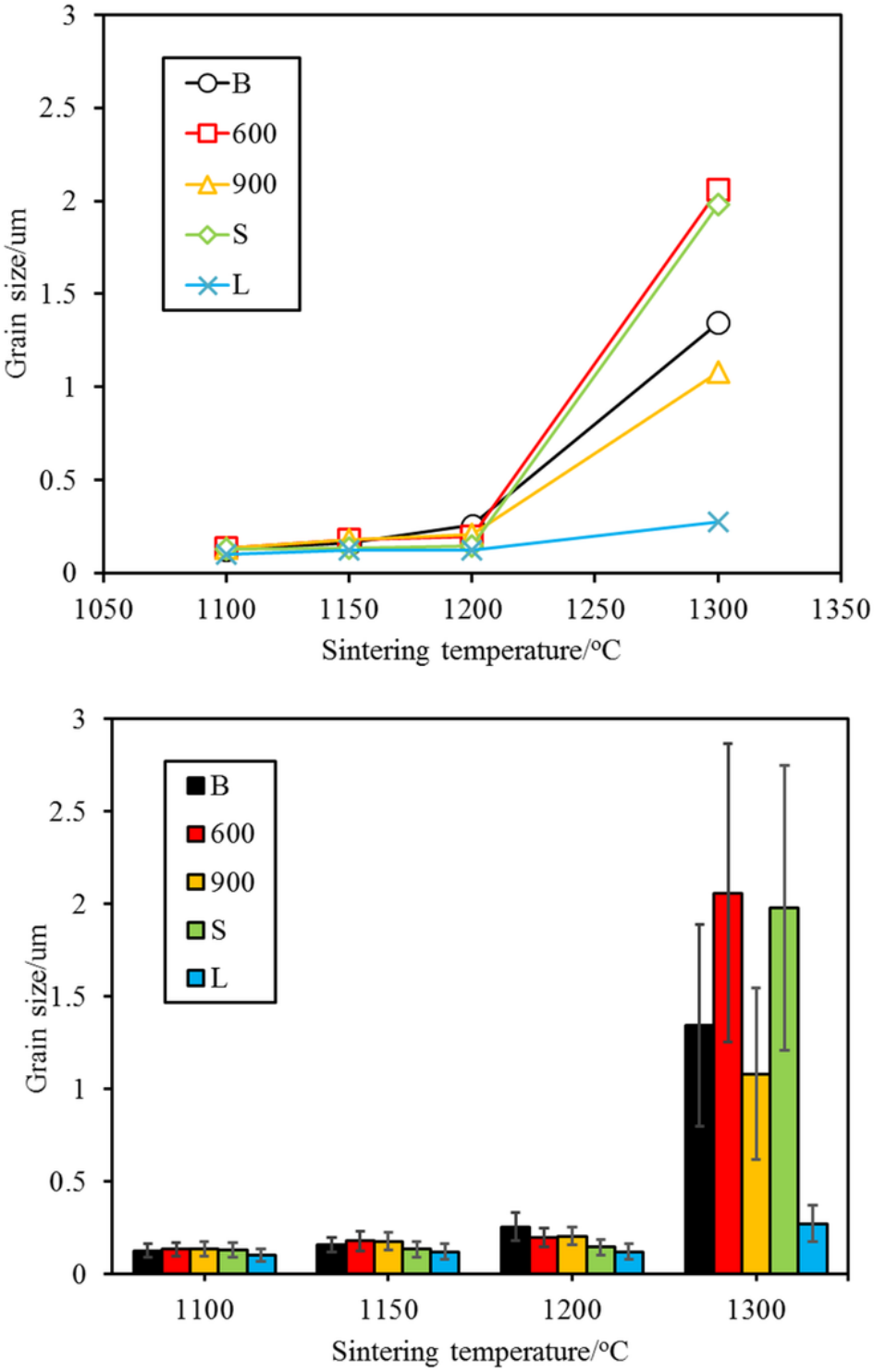

Figure 4

The grain size of samples sintered at different temperature with different pressure applying timings

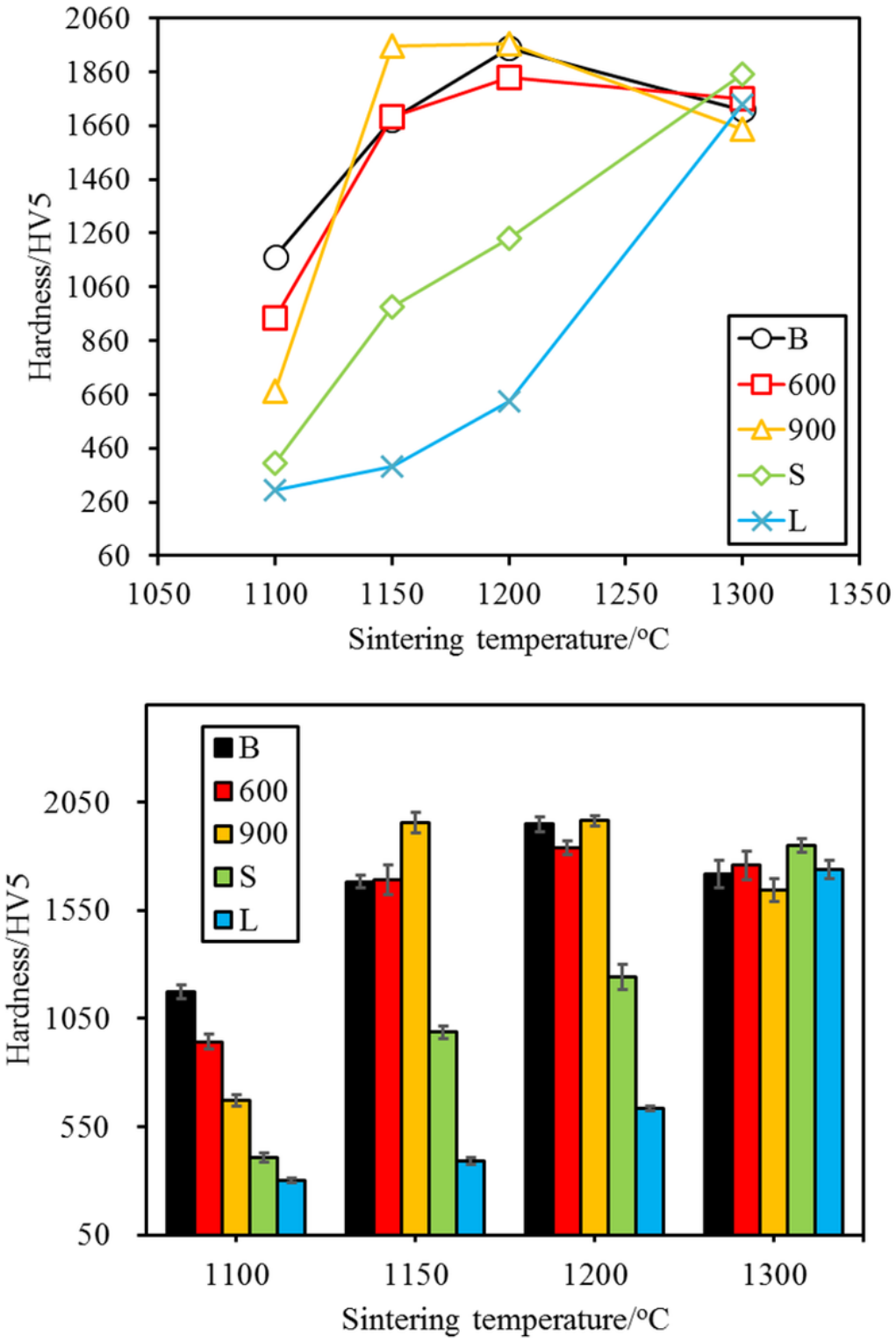

Figure 5

The hardness of samples sintered at different temperature with different pressure applying timings

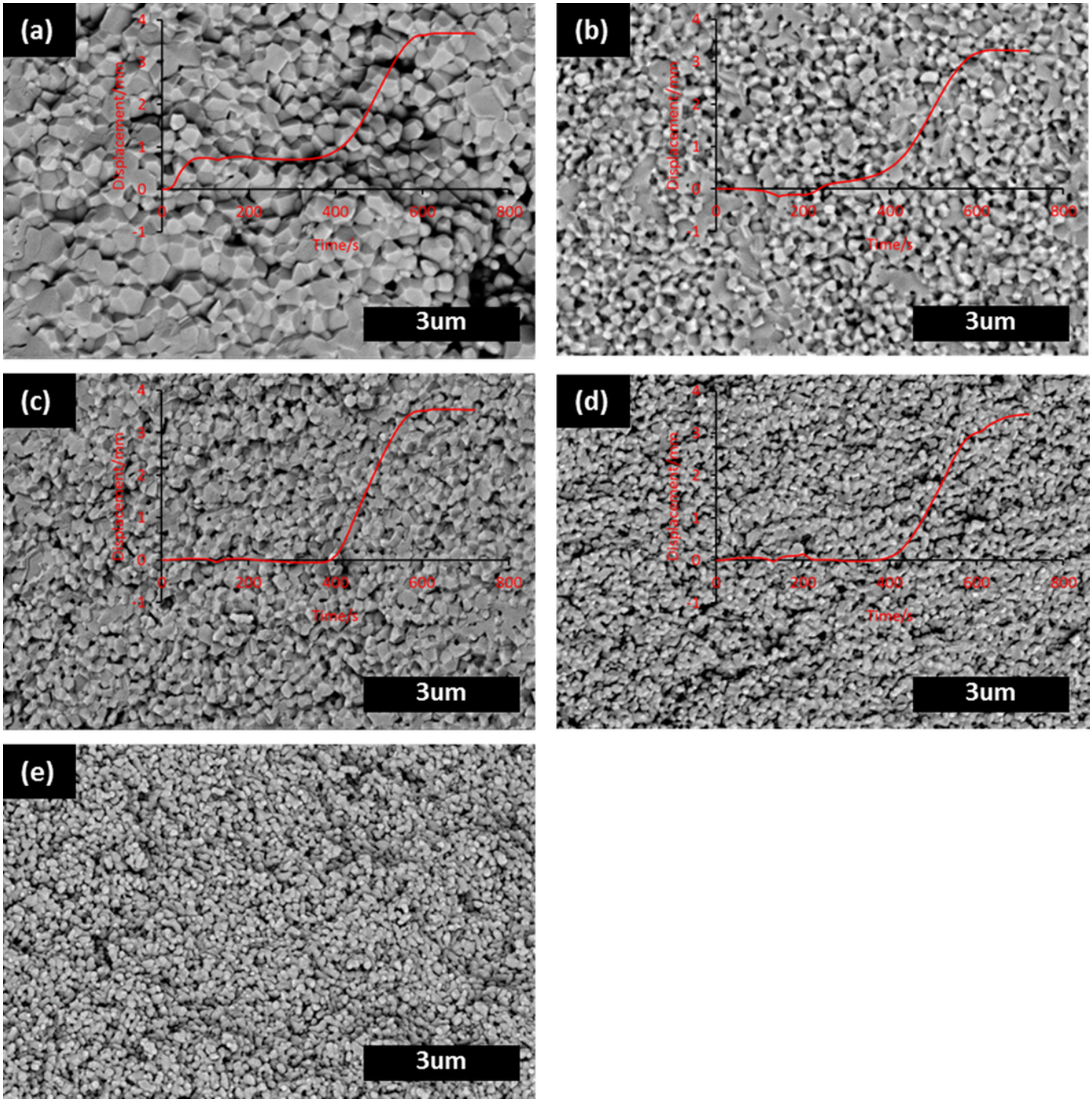

Figure 6

Microstructures and recorded displacements of samples sintered at 1200°C with different pressure applying timings (a) PB-1200, (b) P600-1200, (c) P900-1200, (d) PS-1200 and (e) PL-1200.

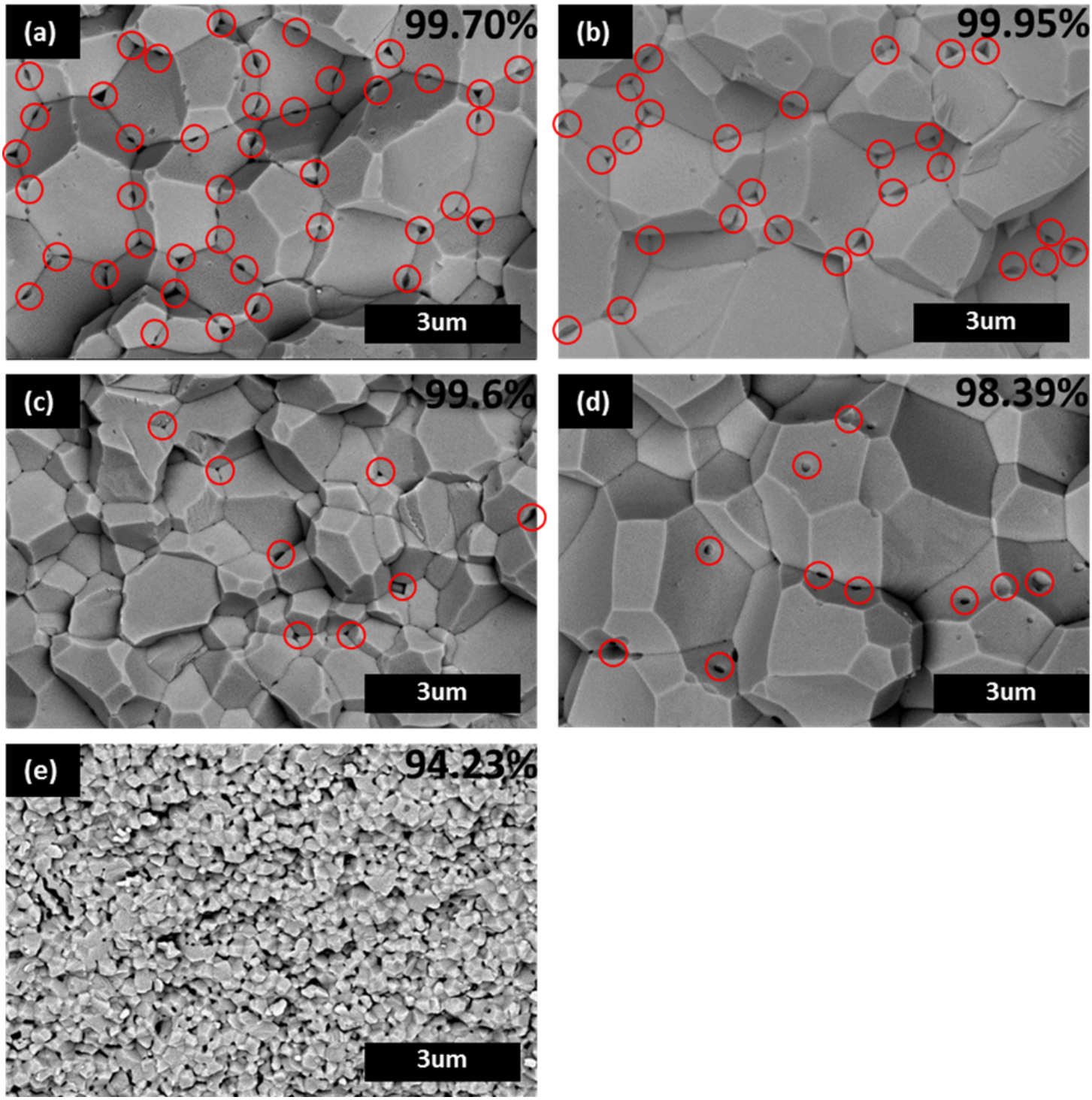

Figure 7

Microstructures and densities of samples sintered at 1300℃ with different pressure applying timings (a) PB-1300, (b) P600-1300, (c) P900-1300, (d) PS-1300 and (e) PL-1300

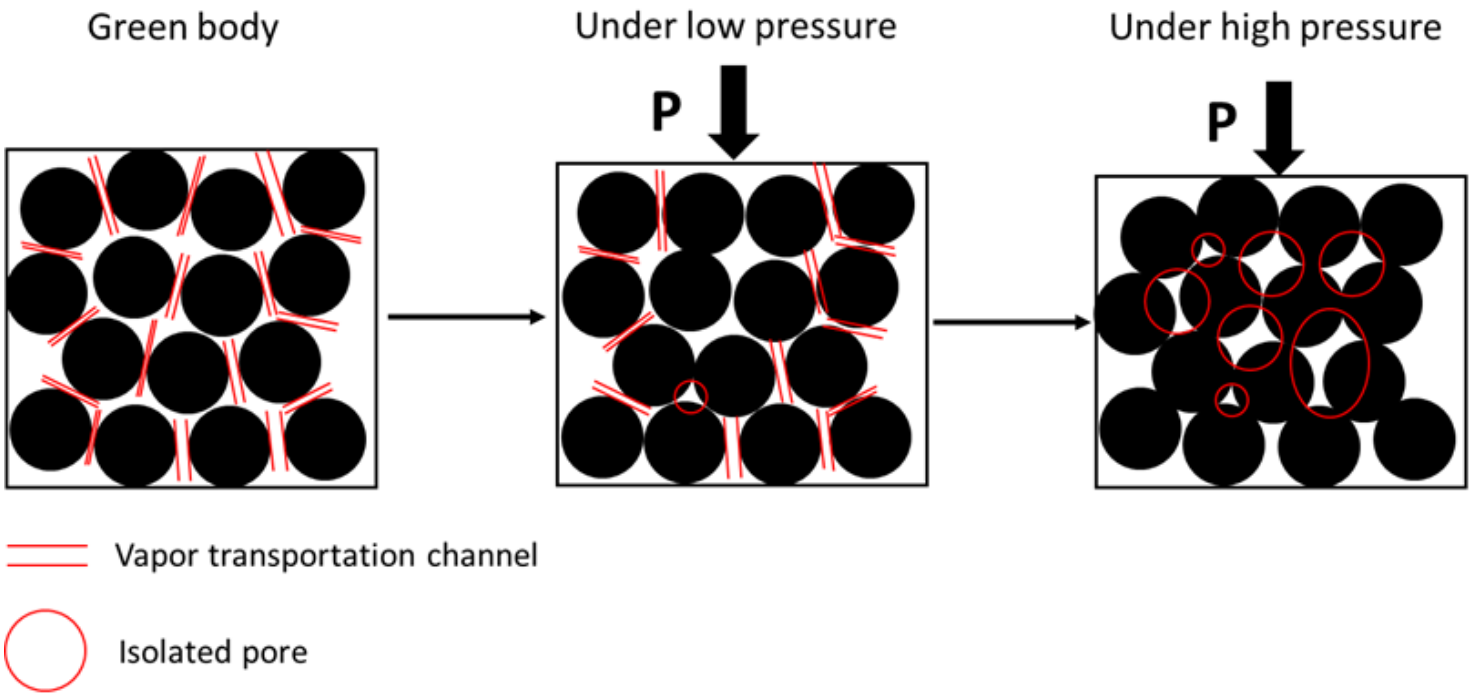

Figure 8

The schematic of blocking vapor transportation channel and making isolated pores under pressure

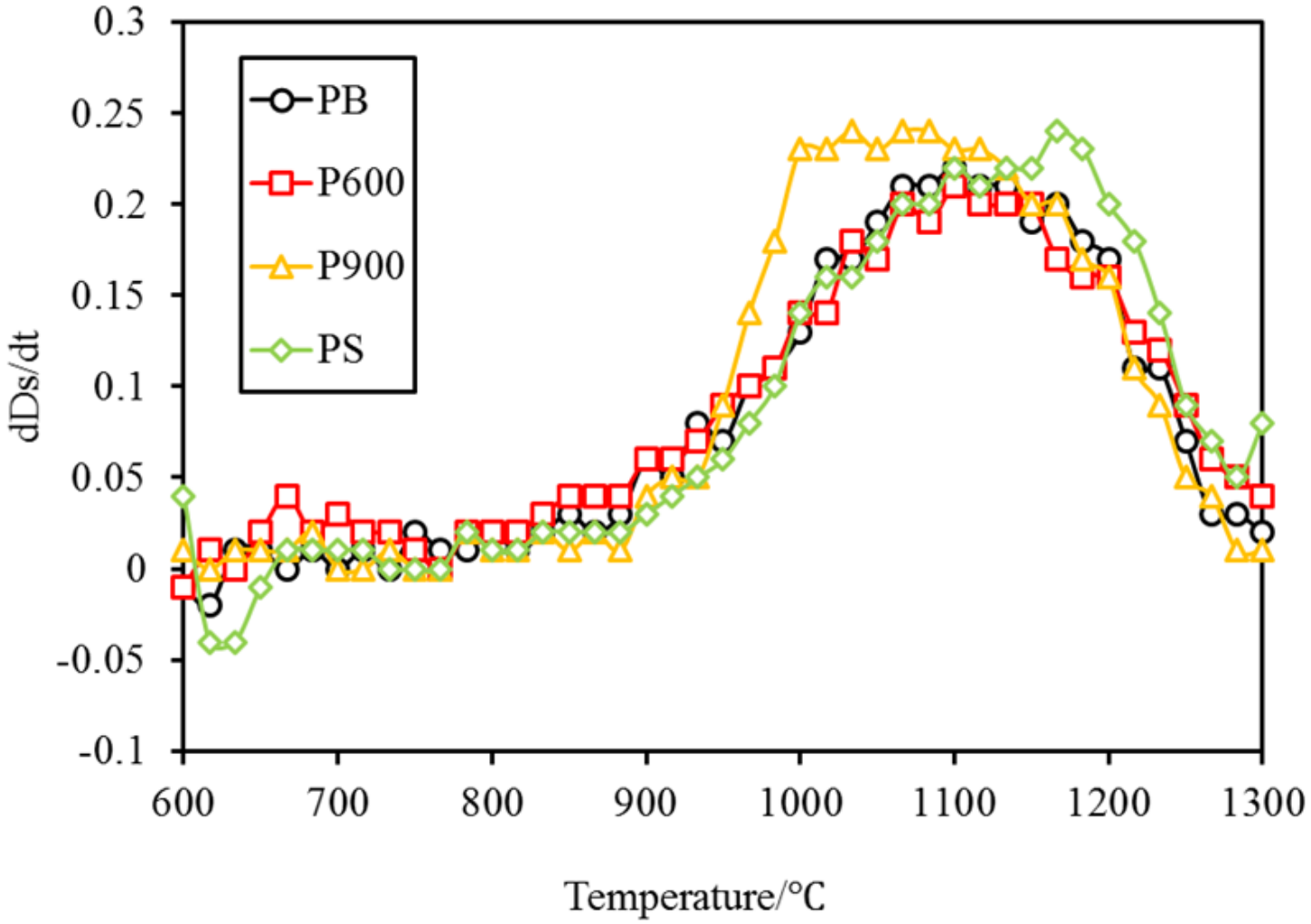

Figure 9

True shrinkage rate of PB, P600, P900 and PS sample sintered at 1300 ℃